Impacts of the inclusion of folded geogrids on the load-settlement behavior of strip footing overlaid fine sand

Hussein Ahmad (houssein.ah@gmail.com)
SBU

Research Article

Keywords: strip footing, geogrid folded, geogrid planar, fine sand, bearing capacity, settlement

Posted Date: January 21st, 2022

DOI: https://doi.org/10.21203/rs.3.rs-1197314/v1

Abstract

This paper describes experimental studies on a strip footing overlaid with unreinforced, planar geogrid-reinforced, and folded geogrid layers of fine sand subjected to static loading. The footing settlement was determined for plate loading of over 25 kN. The variables are assessed in the testing program, including the number of planar geogrid layers, the position of the folded geogrid within the soil, the thickness of the geogrid folded layer, wraparound lap and overlap lengths of a folded geogrid, the spacing within geogrid folded layers, and several geogrid layers. The results indicated the superiority of footing performance as a result of static loading for geogrid folded reinforced sand compared to planar geogrid reinforced sand. In addition, a critical region was found at a certain depth under the footing, where a geogrid folded results in increased footing settlement. This critical area affects the behavior of sandy soils with low footing widths. As a result of static loading, the soil compacts within depth, and sand particles penetrate between the geogrid apertures. Then, they accumulate in a specific area inside the folded geogrid; therefore, they cause small gaps that lead to the rotation of the strip footing in the soil at the foundation surface. In total, based on the results, the reinforced soil-footing systems with adequate folding geogrid layers behave much stiffer; thus, they can handle higher loads with lower settlement than those in planar reinforced soil. Additionally, the results show that the embedment depth and thickness of the folded geogrid are 0.41 and 0.2 of the footing widths, respectively. Consequently, the settlement rate is significantly reduced by increasing the number of folded geogrid layers. The findings revealed that the wraparound technique solution for reinforced cases considerably improves the bearing capacity, reduces settlement, and uses in tight bed spaces.

1. Introduction

The construction of expensive deep foundations can be avoided by utilizing geosynthetic layers within the soil bed as a very cost-effective method. There are numerous studies on the effects of various parameters and variables involving the enhanced performance of reinforced soil via experimental and numerical methods for various ground types. Binquet and Lee (1975) performed a systematic study for the first time to enhance the bearing capacity of strip footings utilizing metallic strips. Then, several papers were published on improving the load-carrying capacity of shallow foundations overlaid a reinforced soil, with different arrangements of reinforcing materials for some sample geogrids (Akinmusuru and Akinbolade 1981; Khing et al. 1993; Guido et al. 1986; Das and Omar 1994; Shin et al. 1993; Omar et al. 1993a; Yetimoglu et al. 1994; Das et al. 1994; Adams and Collin 1997; Sitharam and Sireesh 2004; Patra et al. 2005; Shin et al. 2002; Ghosh and Bera 2005; Basudhar et al. 2007; Chung and Cascante 2007; Latha and Somwanshi 2009; Abu-Farsakh et al. 2013; Kumar and Sahoo 2013; Chen and Abu-Farsakh 2014; Badakhshan and Noorzad 2015; Chen et al. 2021). According to the consequences of these studies in the literature, the settlement characteristics and final bearing capacity of the ground can be enhanced by introducing reinforcements in the soil within a definite depth beyond which no substantial enhancement occurs. Moreover, to improve the effectiveness of geosynthetic reinforcements,

innovative methods have been presented within the literature, such as installing reinforcement multilayers, presenting a granular soil layer above the reinforcement, utilizing a geocell mattress reinforcement system, and utilizing folded geosynthetic methods (Dash et al. 2001; Avesani Neto et al., 2013; Aria et al. 2019a; Hegde and Sitharam, 2015; Kazi et al., 2015a; Biswas et al., 2016; Wang et al., 2018; Raja and Shukla 2020; Ahmad and Mahboubi, 2021).

All the previous works are finally associated with an enhancement in the soil bearing capacity utilizing reinforcing substances. It is deduced that various factors changed the soil bearing capacity, such as the kind of reinforcing substances, soil density, texture, and ratios of various parameters of geosynthetic materials, including reinforcement layers, the position of the geosynthetic first layer, the vertical spacing between consecutive reinforcement layers, the geogrid layer width and the footing depth. In the abovementioned studies, it was revealed that reinforcing the sand increases the footing's ultimate bearing capacity. Normally, this increment is determined in a nondimensional form, BCR, known as the bearing capacity ratio and determined by the ratio between the unreinforced and reinforced footings' ultimate bearing capacity.

As mentioned, the geosynthetic material was utilized as a multilayer or single layer laid horizontally within the soil bed. Practically, under site circumstances, it is not occasionally allowed to use a larger width of the geosynthetic element within the soil layer. To overcome this issue, a modern method is proposed by the authors in this work, including a fully or semifolding reinforcing layer to conform to the architectural and engineering dimensions of the foundation. This new method also provides high soil tolerance and reduces settlement and rotation resistance compared to the normal horizontal reinforcement behavior. The above literature (Kazi et al., 2015a and Aria et al. 2019a) indicates a large lack of complete studies on the performance of footings overlaid with reinforced soil for two different footing widths and another type of geosynthetic. Ahmad and Mahboubi 2021 studied the concept of folded geogrids as semi- or fully folded shapes according to strain analysis. This new technology assists in confining the soil under the shallow footing with an opposite (as bound sand material) length where the settlements and strains become very small while achieving the ideal increase in the bearing capacity of the soil. Hence, to build a more serious comprehension of this performance, in this research, a series of experimental study tests were conducted to assess the behavior of two strip footing widths in reinforced dense sand with geogrid reinforcement.

2. Experimental Analysis

To demonstrate the capability of the proposed method, it is essential to provide laboratory tests for this innovative procedure. and the characteristics of the experimental studies present:

2.1. Description of Soil material

Firozkoh sandy soil with fine grains (No.151) was utilized in the laboratory tests (Ahmad et al. (2020) and Ahmad and Mahboubi, 2021). Sampling of the soil was performed from the Tehran mountainous area in

northeastern Iran. The soil classification ASTM D422 standard was used to analyze the grain size utilizing sieves of various mesh sizes. The obtained laboratory results are Cu=1.90, C_C=1.11, d_{50}=0.34 mm, d_{10}=0.20 mm, d_{min}=0.01 mm, and d_{max}=0.60 mm. Through the Unified Soil Classification System (USCS) and based on Table 1 and Fig. 1, this soil is classified as poor-graded sandy soil (SP). Determining the soil's dry unit weight was oriented by the standard ASTM D2049 utilizing a 0.5" funnel along with the standard Proctor test where the mold height and diameter are 107.0 mm and 151.6 mm, respectively, and the minimum dry density (γ_{dmin}) of the soil was 14.09 kN/m^3. Through the vibrator table test, the maximum dry density (γ_{dmax}) was determined in the same size of mold while obtaining γ_{dmax} of 16.61 kN/m^3 taking into account the specific gravity as G_s=2.68. Figure 2 represents the SEM analysis of particle size. Through six direct shear tests, the mechanical features of fine sand and the geogrid-sand interaction coefficient were determined. The direct shear test is carried out using a 60 × 60 mm mold based on ASTM D5321 at relative densities of 90%. The obtained C, $\phi_{risdual}$, and ϕ_{peak} values were 12 kPa, 32.3°, and 37.5°, respectively (Figure 6). The test Oedometric modulus was acquired from the 1-dimensional experiment within a dry state as an elasticity value of E_{oed}=30 MPa.

2.2. Reinforcement element

Ahmad et al. (2020) used one type of geogrid named CE161 made by an Iranian company. It has a unit weight of 0.70 kg/m^2, a thickness of 3.3 mm, and an opening geometry of 10 mm × 10 mm. The ultimate tensile strength was evaluated at approximately 6.1 kN/m. In all directions, the geogrid possessed the same tensile strength. The specifications of the reinforcement substance presented by the manufacturer are summarized in Table 2. Fig. 4 demonstrates the tensile strength of this kind of geogrid. The geogrid's physical properties are defined in terms of isolation test conditions (ASTM D 4595, 2011).

2.3. Model footing

Here, physical modeling of the footings was performed using two-strip footings constructed of steel plates. The foundations' thickness was 20 mm; hence, it is considered a solid plate not subjected to the scale effect. These two footings have widths of 100 and 75 mm. The direction length of the strip footing (390 mm) is the same as that of the laboratory model box. Through an adhesive coarse sand layer, the foundation bottom surface becomes rough utilizing epoxy glue to ensure uniform roughness in all the tests. At the center of the steel plate, loading is carried out.

2.4. The experimental process and test arrangement

The model experiments were conducted in a large cubic box made of steel with a height, width, and length of 800, 400 mm, and 1400 mm, respectively. Selecting the box's horizontal plane was based on the plane strain problem conditions. The length of the model to the footing width ratio of 16 is considered adequate to prevent interference with the failure surfaces with the model side dimensions. Likewise, the soil bed height in the steel box was chosen as 800 mm. The width of the box and footing was equal. Moreover, the footing length decreased by 5 mm from each side to prevent contact footing with the

sandbox wall. An air pressure of almost 10 bars was provided using a pneumatic cylinder armed with an air compressor as a loading system. By employing the pressure circumstances to the soil sample, the system can secure a steady periodic load. Through a 5-ton capacity jack, the soil load is employed to acquire the soil marginal tolerance in all tests. To calculate the applied force, a load cell was used, and two linear variable differential transformers (LVDTs) were utilized to measure the footing settlement. The test technique was conducted based on ASTM D 1196 (2016), where the load measurements were run and held continuously for 3 min until the settling rate was less than 0.03 mm/min. To prepare the sample, the rain sandy soil technique (Kolbsuzewski, 1948; Kazi et al., 2015a; Ahmad and Mahboubi, 2021) was utilized to attain the regular placement of the soil in the steel box proportional to the needed relative density. The preferred relative density values were obtained by calibration of the sand particles' fall speed and fall height through several trials in a particular aluminum cup. Using a tamper, the appropriate soil unit weight was acquired. The unit weight and relative density of fine sand are 16.46 kN/m^3 and 90%, respectively. The former studies concentrated on dense sandy soil behavior. Since there is no information or laboratory data regarding dense sandy soil, it is essential to perform this study on a high compaction ratio to represent the soil performance. Fig. 5 schematically illustrates this system. Table 3 and Fig. 6a summarize the explanations of the model experiments utilized in the results for planar geogrids. Table 3 and Fig. 6b represent all tests of this study schematically for a folded geogrid.

3. Results And Discussion

Various load experiments were performed on strip-model footing over geogrid-reinforced dense (Dr=90%) fine sand beds. As stated earlier, the load tests principally contributed to determining the outcome of the geogrid wraparound on the settlement performance of the strip footing overlying a fine sand bed. The investigated parameters were the load-bearing capacity for each test arrangement and the settlement (s) of the strip-model footing normalized by its width (B). The load-carrying pressure against the settlement plot was attained from the load test data that are discussed in the following. The strip footing performance on the utilized soil in the plane strain circumstances was assessed by employing 37 experimental tests on the mentioned physical model in Fig. 5. Here, the load is applied continuously to reach the failure with the final settlement magnitude once establishing the failure. The vertical settlement of the footing is stated in mm, and the results curves are plotted by both the applied stress and relative settlement (s/B%). Utilizing a nondimensional factor (BCR), the effect of enhancement was measured through reinforcement layers on incrementing the bearing capacity ratio of the strip footing overlaying a reinforced soil. The parameter BCR denotes the ratio of a reinforced soil bearing capacity to the final bearing capacity of an unreinforced soil (Eq. (1)), by (Badakhshan and Noorzad, 2015; Xu et al. 2019).

$$BCR = \frac{q_{u\,(reinforced)}}{q_{u\,(unreinforced)}} \qquad (1)$$

In the current work, a novel parameter called the increased bearing capacity ratio (BCR_I) is inserted. Eq. (2) represents the ratio of the final load in the geogrid folded reinforced system to that in the system

without folding (i.e.,). planar) reinforced system at a certain settlement.

$$BCR_I = \frac{q_{u\,(reinforced-folded)}}{q_{u\,(reinforced-unfolded)}} \quad (2)$$

Based on Eq. (1), the parameter BCR_f is utilized to measure the bearing capacity ratio of a strip footing overlaying soil with the inclusion of a folded geogrid, as given in Eq. (3):

$$BCR_f = \frac{q_{u\,(reinforced-folded)}}{q_{u\,(unreinforced)}} \quad (3)$$

where q_u denotes the ultimate bearing capacity.

3.1 The optimum length of the reinforcement layers

The current work explains the final bearing capacity utilizing the breakpoint technique. Previous surveys revealed the elastic performance of loose sand owing to the applied load allocation technique; a relative settlement of (s/B)=1% was achieved, equivalent to a 100 kPa limit applied pressure (Fig. 7). Regarding a wedge split in total settlement owing to the increased applied stress and applicable load, a nonlinear elastic model is established by passing a relative settlement of (s/B)=10%, for which the breakpoint is similar to the final failure load. The settlement continues at the breakpoint until the resistance is suddenly reduced, revealing the plastic performance of loose soil. Fig. 7a represents the results for analyzing the determination of the reinforcement length. Their performance utilizing other parameters was characterized through various tests with one geogrid reinforcement layer. Over the tests, the profoundness of the first support layer under the loading plate was also kept constant at u=0.3B. The parameters above were optimal based on the literature review. The applied pressure-based settlement curves obtained from the above four tests behaved approximately differently. The reason is that the plate footing gradually loaded until reaching a definite settlement. Loading continued upon this settlement, and by obtaining identical settlement values, the tests were stopped (an ultimate settlement that causes failure in soil mass). Fig. 7a represents the applied pressure-relative settlement curves for L= 3B, 5B, and 7B for the geogrid planar arrangement. It can be concluded that the applied pressure-relative settlement curves are affected by even a geogrid planar length equal to three times the footing width. For these L/B ratios, at the break point, even a bearing pressure takes place where the slope of the applied pressure-relative settlement curves is changed. An increase is observed at each percentage relative settlement ratio (s/B%) in the strip footing bearing capacity ratio (BCR) for s/B=10 and 11%. According to Table 4, the BCR increases by increasing the geogrid layer length. BCR nonlinearly increases with geogrid planar length until L=5B, after which the geogrid length is not further influenced by the BCR values. L=5B is the geogrid reinforcement optimal length at every relative settlement ratio (Figure 7b). Based on the results of Fig. 7 and Table 4, utilizing a geogrid planar length of 5B can lead to a greater resistance within the reinforced soil system, mostly affecting the geogrid reinforcement. Similar behavior is presented in the next figure (Fig. 7b) for a footing width of B=7.5 cm.

3.2. Effect of multilayers of planar geogrid

Various tests were carried out with these depth ratios (h=0.4B and u=0.3B), the same length ratio (L=5B), and at the same relative density (Dr=90%) to account for the effects of the multilayers of planar geogrid on the bearing capacity for two different strip footing widths B=10 cm and B=7.5 cm. It is assumed that the multilayers of the planar geogrid (N) are within 1 to 3. The applied pressure against the settlement ratio is displayed in Fig. 8 and Fig. 9 for B=10 cm and 7.5 cm, respectively. Not only was their behavior dissimilar, but the slope of the applied pressure–settlement ratio plot also altered with the number of planar geogrid layers for both strip footing widths. For both strip footings, according to the results from Table 5, it was indicated that at the final load, the bearing capacity ratio was the highest when the number of geogrid planar layers was N=three. Therefore, the BCR has been incremented by the enhancement in the number of geogrid planar layers. Figures 8 and 9 and Table 5 confirm the considerable increment in the bearing capacity of the footings with multiple layers of planar geogrid. Incrementing multiple layers of planar geogrids increases the interaction area and their interlocking with sand particles. Thus, shear stresses and larger displacements were created in the soil bed underneath the footing and conveyed by geogrid planar layers to a larger contact mass of the soil bed. Thus, the failure wedge increases, and the frictional resistance on the failure planes becomes larger. Regarding the applied pressure-settlement ratio curves for the reinforced and unreinforced tests, it is indicated that local shear failure is the failure mode for a small strip footing (B=7.5 cm). In the large strip footing (B=10 cm), the unreinforced and reinforced tests contain different failure mechanisms. In the tests with no planar geogrid layers, incrementing the applied pressure, the failure mode remains constant (local shear failure); however, for the tests with planar geogrid layers, the failure mode alters by incrementing the applied pressure to general shear failure. In other words, for a large strip footing (B=10 cm), planar reinforcement layers are more pronounced than for a small strip footing (B=7.5 cm). According to the experimental results, the main cause for the largest increment in final bearing capacity in the large strip footing compared to the small strip footing under the same test conditions may be ascribed to the reinforcement mechanism limiting the lateral and spreading deformations of the soil. A larger mobilized tension is caused by the large strip footing in planar reinforcement layers supporting the reinforcement for resisting the imposed horizontal shear stresses created in the mass under the loaded area by transmitting the footing load to deeper soil layers. Thus, the failure wedge and consequently the frictional resistance on failure planes become greater. The discussion in this section will be utilized to compare with the other results of the strip footing resting on folded geogrid layers. Table 5 presents the results of the strip footing test for two footing widths (B=10 cm and B=7.5 cm) in both unreinforced and planar reinforced soils.

3.3. Effect of one geogrid folded layer

Currently, geogrid folded methods (GFMs) have become widely used as reinforcing elements in many geotechnical installations, including dams, embankments, slopes, roads, bridges, beneath shallow footings, stone columns, and others, by Shukla and Yin (2006). Geogrid wraparound methods have rarely been applied to soil reinforcement underneath shallow foundations. Nevertheless, there are advantages

to using a quality-controlled geogrid folded as a reinforced soil bed. The advantages of folding a quality-controlled geogrid may be investigated as follows:

3.3.1. Optimum lap length

A series of bearing capacity tests were conducted on a fine sand bed to develop a new reinforcement method that is dissimilar from traditional reinforcement methods. Traditional methods usually place reinforcing materials (geogrids, geotextiles, geonets, etc.) horizontally into foundations (Binquest and Lee, 1975; Omar et al., 1993b; Huang and Tatsuoka, 1990; Adams and Collin, 1997; Das et al., 1994; Lee et al. 1999; Shin et al. 2002; Chen et al., 2013; Ahmad and Mahboubi, 2021). Part of the geogrid was folded around the end with the lab length (//L=0.25 and 0.5) and embedded at different depths in the soil bed. The second technique is geogrid full folded with a lap length (//L=0.75 and 1.0). However, the result of the trial in the traditional planar way (L/B=5) has been used to compare it with the new technique results. The mechanism of the reinforcement was investigated through the observation of the applied pressure-settlement curves. One geogrid layer of length L=5B=50 cm is placed horizontally in the soil bed at a depth of u=0.3B=3 cm below the ground. The test only proves a substantial increment in bearing capacity, which is due to mobilized tensile stress at the soil-geogrid interaction, distributed vertical stress at a wider width, and transferred it to deeper depths in the soil mass. However, the settlement of the strip footing increases with increasing applied load. Agreeing with the theory of elasticity, the minor principal strain ε_3 or the major tensile strain takes place almost along the direction of the minor principal stress σ_3. It is expected that placing geogrid-reinforced materials along the direction of the minor principal strain ε_3 would be the most efficient means to reinforce foundations. This is because the geogrid reinforced material should be placed in the most extendable direction where the material may develop maximum tensile deformation. Therefore, it is placed at embedment depth (d=0.2B=2 cm and u_f=0.3B=3 cm) by closing a part of the geogrid around the end with lap length *l*=0.25 L=12.5 cm. As anticipated, the bearing capacity of the reinforced soil is incremented owing to the frictional resistance between the upright element of the folded geogrid and the soil particles. Nevertheless, the increase is not enough because the soil particles move upwards from the two positions of the footing, and failure occurs as local punching shear. To overcome this problem, both sides of the geogrid folded underside of the footing with lap length *l*=0.5 L=25 cm and placed at embedment depth (d=0.2B=2 cm and u=0.3B=3 cm) can be offered. As a consequence, the holding capacity increases dramatically, and the settlement ratio decreases. When the lap length is extended to (*l*=0.75 L=37.5 cm and *l*=1.0 L=50 cm) and shares two sides of the lap length with them, the bearing capacity is more significantly improved, and the settlement is much smaller than that measured in geogrid planar layers. Because two sides of the lap length are shared and fixed with them, an additional tensile force induced in the geogrid folded, and additional lateral resistance affected the behavior of the strip footing on the reinforced sand. The mechanism of support is experimentally investigated in the following images. It can be understood that a large slip line is generated under the geogrid folded layer. This is because when the external load is applied on the strip footing, the wrapped material behaves as part of the footing. To explain the largest bearing capacity in a full geogrid folded state, a close look at the geogrid wrapped embedment in fine sand underneath the footing subjected to

strip loads is needed. The width of a geogrid folded rectangular shape is increased up to several centimeters due to lateral expansion. Moreover, the soil inside the wrapped geogrid seems to have been more densified and solidified, as if it was integrated with the footing. The external force applied on the footing induces a tensile force along with the geogrid layer as a result of the reinforcement extension. The soil particles within the folded geogrid are restrained, leading to an increment in the vertical effective stress. Later, the shear strength of the soil particles increases. As part of the footing, the solidified system (soil-geogrid folded) thus greatly increases the bearing capacity of the foundation. This theory is analogous to the increase in normal strength (N) leading to an increase in friction force F=μN. It is concerned that the hypothesis implies a “reversal idea” of applying an external force to reinforce foundations, which was ordinarily the “enemy” of institutions. Figure 10 presents the observational study results of the plate load test (PLT), in which it describes the settlement ratio (%) of the strip footing relative to the applied force per unit area. According to Figure 11 and Table 6, the ultimate settlement ratio and BCR_f of the footing for a geogrid planar layer (L=5B) are 12% and 1.47, for folded geogrid (*l*=0.5 L) are 6% and 1.55, for folded geogrid (*l*=0.75 L) are 4% and 1.56, and for folded geogrid (*l*=1.0 L) are 5% and 1.58. Therefore, the new technique has a large effect on asperity settlements of the footing and deformation of the soil layer. Therefore, the soil particles inside the geogrid folded element do not have a relative motion to the footing. Likewise, a wedge failure sandwich-shaped zone is made beneath the geogrid wrapped system. It seems that this new system has integrated with the strip footing to form a wider and deeper footing. This observation explains the effect of additional confinement strength by the inclusion of folded geogrids. Table 6 denotes the results of the strip footing test for footing width (B=10 cm) in both unreinforced and geogrid folded reinforced soils.

3.3.2. Optimum depth for geogrid semifolded

Among the vital parameters for reinforced soil with semifolded geogrids is the reinforcement layer embedment depth from the soil surface. Various results have been reported (u) in planar geogrid reinforcement under strip loading conditions. Researchers have highlighted the critical values for (u) beyond which further increment has no effects on bearing capacity, as stated in the previous section. For the geogrid folded system, five different depths (d=0.1B- 0.2B- 0.3B- 0.4B, and 0.5B) from the footing bottom are considered for the lap length (upper part //L=0.5) of a single geogrid folded layer (in which the total embedment depths in dimension condition u/B=3, 4, 5, 6 and 7 cm are considered). The thickness of the geogrid folded layer (x=0.2B=2 cm) is proposed. With a relative density of 90% and B=10 cm. The results of the applied pressure versus settlement ratios of one layer of folded geogrid are represented in Fig. 12. It is found that the depth ratio of u=0.4B gives the highest final bearing capacity and lower settlement amount.

Hence, it can be expressed that semifolded geogrids are more effective in reinforcement based on an increase in the final load-bearing capacity when installed in dense sand beds at D=0.4B. Figure 13 represents the changes in the subgrade reaction modulus (k_s) with an embedment depth ratio (u/B) for geogrid semifolded sand beds with Dr=90%. According to Fig. 11, the load-bearing pressures equivalent to settlements of 1.25 mm and 2.00 mm and the ultimate settlement at failure are determined

for reinforcement with geogrid wraparound end conditions. It is found that by increasing u/B, k_s continues to increase until u/B=0.41; then, it decreases by increasing u/B for the reinforced case with the geogrid semifolded at all relative settlements. Moreover, for u/B=0.41, the geogrid semifolded increases ks by approximately 13800, 11000, and 11685 kN/m^3 for settlement ratios s/B%=1.25, 2.00, and final settlement (s_u%), respectively. Therefore, semifolded geogrids are more advantageous based on increasing the subgrade reaction modulus when installed in very dense sand beds at u=0.41B. It was indicated that a lower footing settlement is significantly obtained by any applied load-bearing pressure and the semifolded ends in comparison to the planar reinforcement case. The improvement is mainly caused by the confinement effect resulting from the folded method, Shukla (2004) and Shukla (2016). Thus, the geogrid reinforcement should always be installed in dense to very dense sand appropriately possessing geogrid semifolded ends to reach the highest effectiveness based on increasing the modulus of the subgrade reaction and final load-bearing capacity. Moreover, it is worth noting that a relatively lower land width is required for this installation technique to construct the reinforced soil foundation bed.

Figure 14 illustrates the impact factor (IF) variation with the embedment depth ratio (u/B) for reinforced soil with a relative density of 90% for a one-layer reinforcement located at various depths with a semifolded geogrid. It is worth noting that IF_u does not denote the same as $IF_{1.25}$ and IF_2, in which the subgrade reaction modulus is defined as ($IF_u=K_{su}/K_{un}$, $IF_{1.25}=Ks_{1.25}/K_{un}$ and $IF_2=Ks_2/K_{un}$) for folded geogrid layers (where k_{un}, k_{su}, $K_{s1.25}$ and K_{s2} denote the subgrade modulus amounts of the unreinforced soil, the folded-reinforced bed at an ultimate settlement ratio, the folded-reinforced bed at a 1.25% settlement ratio and the folded-reinforced bed at a 2% settlement ratio, respectively). The IF_u is an enhancement factor utilized by Latha and Somwanshi (2009). They found that the IF increments by increasing the embedment depth of the case with a geogrid semifolded for all three relative settlement ratios. It is worth noting that for any settlement ratio, IF_u is always greater in the case of reinforcement with geogrid semifolded at u/B=0.41. For instance, for s/B=1.25%, the wraparound increments IF by approximately 1.73 in comparison to the case with no reinforced layer for Dr=90%. For s/B=2%, the corresponding value is 1.57. Therefore, the results dictate that the semifolded method is highly effective in the case of very dense conditions.

3.3.3. Effect of multilayers of geogrid semifolded

Here, the effects of vertical spacing between geogrid folded layers (*h*) on the load-bearing capacity of footings were assessed utilizing the optimal u/B, d_1/B, *l*/L_1, and Dr values of 0.40, 0.2, 0.5, and 90%, respectively. The total embedment depth for each layer is computed as (D=u+ (h+x) ×N, in which $u=d_1+x$ and $d_2=u+h$). where d_1 and d_2 are the embedment depths of the lap folded element for the first and second geogrid folded layers, respectively. The details of the layout are shown in Fig. 6b. The variation in BCR, as h/B, is constant for the second and third layers (Fig. 16). It was found that by the bearing capacity of the reinforced footing, the optimal value of vertical spacing is obtained between geogrid folded layers at h/B = 0 for a relative density of 90% and gives a greater bearing capacity ratio of BCR_f=2.22 for both and three reinforcement layers. Fig. 15 shows the change in compressive

stress with their equivalent displacement at a relative density of 90%. The curves reveal a peak point for h/B=0 at the second and third reinforcement layers since geogrid layers have induced tensile strengths leading to failure. This means that deformation at the tensile strength of the geogrid is much less than the deformation at the final load-bearing capacity. Moreover, the results revealed no significant difference between the curves at the steps of the first loading (displacement ratio lower than 2%) for geogrid layers with h/B=0.2 and 0.4 values; however, the difference between curves was more obvious at a higher displacement. When h/B=0.0 (no space between geogrid layers), the settlement ratio, confining pressure, and bearing capacity are at their lowest highest and greatest values, respectively. Furthermore, it was found that incrementing the vertical depth increased the confining pressure; however, no considerable difference was found for h/B>0.

For two geogrid folded layers that are embedded at depths D/B=1.2 and 1.8, sudden failure occurs at a certain point at settlement ratios of 6% and 6.6%, respectively. Inclusion strengthens the geogrid folded layer, leading to passive vertical pressure and rearrangement of the stresses between reinforcement layers. Geogrid folding helps with densifying soil, expanding the volume of soil, and remobilizing sand particles around the lap length. This behavior of soil takes place by increasing the bearing capacity and settlement to reach the final failure point, and the failure surface of the soil will lengthen to the ground surface. This failure refers to the occurrence of general shear failure in reinforced soil with two geogrid folded layers. The settlement is lower for a considered applied pressure, with the inclusion of part or full folded layer of the geogrid reinforcement, and is lower again by increasing the number of reinforcement layers. Figure 16 displays that, in general, for constant vertical spaces between the geogrid folded layers (h/B=0.0), more reinforcement layers result in a stiffer foundation. The inclusion of more than two geogrid folded layers had no considerable effect on the increasing load-bearing capacity of footings and reducing settlement. It also did not change the failure mechanism of the soil foundations. Therefore, in this research, the optimum number of geogrid folded layers was achieved as two layers.

3.4. Comparison of the behavior of multilayered geogrid folded and multillayer geogrid planar arrangements

Fig. 17 represents the bearing pressure-settlement behavior of unreinforced soil, geogrid folded and planar geogrid reinforced foundations when the geogrid semifolded layers were placed in N=3, h/B=0, d_2/B=1.0, D=1.2B; N=2, h/B=0, d_2=0.6B, D=0.8B; N=2, h=0.2B, d_2=1.0B, D=1.2B; N=2, h=0.4B, d_2=1.6B, D=1.8B, and planar geogrids were rested at N=2, u=0.3B, h=0.4B and N=3, u=0.3B, h=0.4B, respectively, at a relative density Dr=90%. The lap length and upper depth of laps are kept constant for all geogrid semifolded layers as *l*/L=0.5 and d_1/B=0.2, where L=5B and B=10 cm. It may be found that by incrementing the reinforcement layers (incremented mass of the geogrid folded and geogrid planar reinforcements and subsequent increment in the reinforced zone depth; D/B), both bearing pressure (bearing pressure at a specified settlement) and the stiffness considerably increase. For unreinforced soil (Fig. 17), the peak bearing pressure occurs at a footing settlement equivalent to approximately 9% of the footing width. In the case of planar geogrid layers, the failure points for two and three layers occur at footing settlements equal to 25% and 20%, respectively. On the other hand, for two and

three geogrid folded layers, the peak failure point takes place at a settlement ratio of less than 7% of all multilayered geogrid semifolded layers. This explains the significant effect of inclusion geogrids semifolded in the soil mass bed. For the planar arrangement, over a footing settlement level of s/B=10–25%, a considerable reduction in the pressure-settlement curve slope is observed. In this range of settlement, the upper surface heave became observable by the naked eye with distinct gradient alterations. By ending the test, the obtained results indicated that the heave was attributed to the soil-reinforcement composite material locally rupturing near the footing owing to the larger footing displacement. Over this phase, the pressure–settlement curve slopes for the moderate and heavily reinforced cases remain almost constant although increasing the footing bearing pressure continuously and incrementally as more mobilization of reinforcement and anchorage is activated. In contrast, folded geogrid behaves differently. The settlements are relatively small in comparison with the case of planar reinforcement. The behavior of the folded lap section as an anchorage element helps reduce the deformations and displacements that are accumulated under the surface of the strip foundation and move them horizontally to spread it into the soil (increasing tensile strength and matching lap part with footing leads to get wider strip footing); thus, it leads to an increment in the resistance confining pressure and transferring a portion of the load to be distributed with the depths without an increase in the settlement, and the resistance continues to increase gradually to reach general shear failure.

The behavior of the geogrid folded and planar arrangement in incrementing the bearing capacity of a reinforced sand bed owing to the increased number of geogrid folded layers or in the number of planar geogrid reinforcement layers are given in Table 7. The unreinforced bed and the effect of the bearing capacity ratio variation (BCR_l and BCR_f) can be compared based on the reinforcement layer number. In all situations, the values of BCR_l and BCR_f are larger at failure for folded geogrids than for planar geogrid layers, with multilayered reinforcement as the footing penetrates further. This can be attributed to the tensile strain's greater mobilization in the reinforcement layers and the additional confinement pressure provided between layers by the inclusion of the folded reinforcement. For multilayered reinforcement, no considerable enhancement in performance is attained when more than three (N>3) folded geogrids are used. Therefore, when three layers of folded geogrids are located in d_1=0.2B, h/B=0.0, and u=0.4B, the highest zone of soil usefully reinforces lengthens to a depth of approximately 0.8B (D=0.8B, Table 7). However, Table 7 shows that the performance enhancement caused by the planar arrangement provision may continue beyond 3 layers (N=3 with a reinforcement zone depth of D=1.1B. Table 7 also shows that an enhancement in bearing capacity is greater for the geogrid folded arrangement than for the geogrid planar arrangement, regardless of the settlement ratio of the footing. For instance, for N=2 and a level of settlement ratio of s/B=7%, the geogrid folded installation enhances the bearing pressure for BCR_l and BCR_f by 1.5 and 2.22, respectively, more than the planar geogrid installation (BCR_l =1.13 and BCR_f =1.67). In total, the results demonstrate that the geogrid folded system presents better performance than the geogrid planar system.

3.5. Effects of footing width on geogrid folded system

The effect of another footing width (B=7.5 cm) on the behavior of very dense reinforced fine sand with the folded improvement method was carried out. The constant parameters in this series of tests for the folded system were D=0.6B, d=0.3B, L=5B, and N=1, assuming for planar system u=0.3B, L=5B, and N=1. The variable parameters are only lap length *l*/L=0.25, 0.5, 0.75 and 1.0 (these parameters are *l*=9.375, 18.75, 28.125 and 37.5 cm, respectively). Figure 18 shows the applied pressure–settlement ratio results for unreinforced geogrid layers, one planar geogrid layer and one folded geogrid layer with various lap lengths. The bearing capacity increases with increasing lap length, and this increment is more considerable for lap length increases for full lap lengths *l*/L=0.75 and 1.0 than for semifolded lab lengths *l*/L=0.25 and 0.5. In the case of full folding with a lap ratio *l*/L=1, the curve reached its maximum bearing capacity at a lower settlement than the other three lap lengths. In the three semifolded cases (Fig. 18), the applied pressure–settlement ratio curves first experienced a peak value $q_{ur(1)}$= 220, 175, and 438 kPa for *l*=0.25 L, 0.5 L, and 0.75 L, respectively, at settlement ratio s/B=4.85, 3.67 and 10.21%, respectively, then followed by a sudden decrease in their correspondent bearing pressures and a large increase in settlement ratio with this value s/B=35%, after this step the applied pressure increases with increase in settlement ratio to reach at the second peak pressure values $q_{ur(2)}$= 396, 414 and 560 kPa for *l*=0.25 L, 0.5 L and 0.75 L, respectively, at the largest settlement ratio s/B=42.69, 42.13 and 27.71%, a result of developing a failure surface.

The behavior of the small strip footing (B=7.5 cm) under consideration rests on the folded reinforced sand with dense compaction, and an increment in the applied pressure on the footing will also occur with increasing settlement. Nevertheless, in this case, the failure surface in the soil mass will extend gradually outward from the foundation. When the applied pressure on the foundation equals $q_{ur(1)}$, the foundation movement will be along with sudden jerks (Das, 2019). The failure surface requires a significant movement of the foundation in the soil to prolong to the ground surface. This explains the mechanical effect of the upper part of the geogrid semifolded (lap effect) in which the rupture occurs in transverse and longitudinal ribs. Beyond that point, because of the inclusion of a semifolded geogrid, an increment in applied pressure will be accompanied by a larger increment in foundation settlement. This refers to the performance of the lower part of the geogrid semifolded. The load per unit area of the foundation, $q_{ur(1)}$, is referred to as the first failure bearing pressure (Vesic, 1963). Note that the second peak pressure value, $q_{ur(2)}=q_{ur}$, is referred to as the local shear failure of geogrid semifolded reinforced soil, as shown in Fig. 19b. In contrast, at a larger lap length *l*/L=1 for the full-folded geogrid, the applied pressure–settlement ratio curve reached its peak value (q_{ur}=566 kPa) at a lower settlement ratio (s/B=8.81%) until the failure surface was generated. This behavior is similar to the behavior of the strip footing with a larger width (B=10 cm) at the same relative density Dr=90%.

To determine the optimum embedment depth for strip footing with width B=7.5, a series of experimental tests was performed. The constant parameters in this series of tests for the semifolded system were Dr=90%, L/B=5, and N=1. The variable parameters are only lap depth d/B=0.2, 0.3, 0.4 and 0.5 these parameters with numbers are d=1.5, 2.25, 3.0 and 3.75 cm, respectively, and the total depth are D/B=0.4, 0.6, 0.8 and 1.0 these parameters with numbers are d=3.0, 4.5, 6.0 and 7.5 cm, respectively. Figure 20a

demonstrates applied pressure–settlement ratio results for folded geogrid layer system with various lap embedment depth, and it is observed that the bearing capacity increases with increasing the lap depth, with this increase more significant for a lap depth increase for embedment depth d=0.2B and D=0.4B, than for a semifolded lab length d/B=0.3, 0.4 and 0.5. As a result, the optimum depth for this type of technique is d/B=0.2 and D/B=0.4, in which B=7.5 cm, the footing width. Figure 20b represents the variation in applied stress with their equivalent displacement at a relative density of 90%. Note that when h/B=0.0 (no space between geogrid folded layers), the bearing capacity, confining pressure, and settlement ratio are at their maximum, highest and minimum values, respectively. Furthermore, it was found that incrementing the vertical depth increased the confining pressure; nevertheless, there were no significant differences for h/B>0.

4. Conclusion

Static loading tests were conducted on two shallow strip footings on geogrid-reinforced and unreinforced sand. A small-scale physical model was considered comprising 37 tests. Two tests were performed on the unreinforced sand foundation, and thirty-two tests were conducted on reinforced sand with various reinforcing schemes (planar and semifolded). One type of fine sand with a relative density of 90%, one type of geogrid, two footing widths (B=75 mm and 100 mm), three numbers of LVDTs, ten pressure cells and a steel box are used to carry out the experimental procedure and to comprehend the performance of reinforced soil with the geogrid folding technique. The following concluding remarks are drawn:

1- The inclusion of one folded geogrid could lead to an increase in the ultimate bearing capacity of the footings compared with the installation of planar geogrids. The final bearing capacity ratio BCR_f (the ratio between the final bearing capacity of geogrid folded and unreinforced bed) and BCR_l (the ratio between the final bearing capacity of geogrid planar and geogrid folded bed) could be as high as 1.58 and 1.07, respectively. The maximum increment in final bearing capacity was found in the footing on soil with one layer of geogrid fully folded at the depth of lap 0.2B, lab length *l*=L, and total depth D/B=0.41 for a relative density of 90%. Therefore, the mobilized shear strength at the lap part of the geogrid–soil interface affects the tension effect and performance anchorage of the geogrid folded system.

2- Inclusion of one layer of folded geogrid can greatly decrease the settlement response and deformation in the soil bed. For soils with one layer of geogrid semifolded (*l*=0.75 L), the settlement reduction was most effective in the case of sharing two sides of a lap with them. The inclusion of folded geogrid reinforcement was as effective as incorporating more layers of planar reinforcement based on settlement reduction and bearing capacity increment. By sharing two sides of overlaps with them, the lower lateral strain and lateral confinement are increased by interfacial resistances resulting from the interaction between the soils beneath above the reinforcement and the geogrid folded reinforcement. This increases the elastic modulus of the soil layer and improves the vertical stress distribution on the bed, known as the “vertical stress dispersion effect”, which correspondingly reduces the vertical pressure over the soil bed.

3- The optimal embedment depth to achieve the highest load-bearing capacity and minimum settlement is approximately 0.41B (B is footing width), in which the optimum depth of lap length is 0.2B for fine sand with the largest relative density of 90%. As a result, this embedment depth transfers the stress at a deeper depth inside the soil mass and redistributes the footing load per unit area over a wider area, which is referred to herein as the “stress dispersion effect.”

4- Incorporating more layers of semifolded geogrids greatly increases the foundation soil stiffness, greatly improves the bearing capacity and significantly reduces the foundation settlement. The highest bearing capacity ratio was obtained for optimum numbers of the two layers. The BCR ratios are in the very large limits because the vertical space between layers (*h*) is zero (i.e.,). geogrid folded layers are placed over them directly).

5- The footing width considerably affected the behavior of the strip footing on reinforced soil. Strip static loading on smaller widths changes the footing failure mechanism on geogrid folded reinforced sand: general failure occurs in soils with two layers of geogrid full-folded reinforcement, and local shear failure occurs in the geogrid semifolded cases. As a result, the optimum depth for this type of technique is d=0.2B and D=0.4B, in which B=7.5 cm, the footing width. Note that when h/B=0.0 (no space between geogrid folded layers), the bearing capacity, confining pressure, and settlement ratio are at their greatest, highest and least values, respectively. Furthermore, it was found that incrementing the vertical depth increases the confining pressure; nevertheless, there was no significant difference for h/B>0.

Declarations

Conflict of interest

No conflicts of interest associated with this study and no financial support influencing the results are declared by the authors.

References

Abu-Farsakh M, Chen Q, Sharma R (2013) An experimental evaluation of the behavior of footings on geosynthetic-reinforced sand, *Soils, and Foundations*, **53**, (2), 335–348.

Adams MT, Collin, JG (1997) Large model spread footing load tests on geosynthetic reinforced soil foundations, *Journal of Geotechnical and Geoenvironmental Engineering*, **123**, (1), 66–72.

Ahmad H, Mahboubi A, Noorzad A (2020) Scale effect study on the modulus of subgrade reaction of geogrid-reinforced soil. SN Appl. SCI., 2(4), 394. https://doi.org/10.1007/s42452-020-2150-4

Ahmad H, Mahboubi A (2021) Effect of the interfacial shearing stress of soil–geogrid interaction on the bearing capacity of geogrid-reinforced sand. *Innov. Infrastruct. Solut.* **6,** 57. https://doi.org/10.1007/s41062-020-00430-8

Akinmusuru JO, Akinbolade JA (1981) Stability of loaded footings on reinforced soil, *Journal of Geotechnical Engineering Division ASCE*, **107**, (1), 819–827.

Aria S, Shukla SK, Mohyeddin A (2019a) Behavior of sandy soil reinforced with geotextile layer having partially and fully wrapped ends. Ground Improv. 1–34. https://doi.org/10.1680/jgrim.18.00102.

ASTM D422-63 (2007) Standard Test Method for Particle-Size Analysis of Soils (Withdrawn 2016), ASTM International, West Conshohocken, PA, www.astm.org.

ASTM D5321/D5321 M-19 (2019) Standard Test Method for Determining the Shear Strength of Soil-Geosynthetic and Geosynthetic-Geosynthetic Interfaces by Direct Shear, ASTM International, West Conshohocken, PA, www.astm.org.

ASTM-D2049 (1969) Test Method for Relative Density of Cohesionless Soils.

ASTM D 1196 (2016) Standard Test Method for Nonrepetitive Static Plate Load Tests of Soils and Flexible Pavement Components, for Use in Evaluation and Design of Airport and Highway Pavements. American Society for Testing and Material, ASTM International, Philadelphia, PA, USA

ASTM D 4595 (2011) Standard Test Method for Tensile Properties of Geotextiles by the Wide-Width Strip Method. American Society for Testing and Material, ASTM International, Philadelphia, PA, USA

Avesani Neto J, Bueno B, Futai M (2013) A bearing capacity calculation method for soil reinforced with a geocell. *Geosynthetics International,* 20**,** 129-142.

Badakhshan E, Noorzad A (2015) Load eccentricity effects on behavior of circular footings reinforced with geogrid sheets, Journal of Rock Mechanics and Geotechnical Engineering (2015), http://dx.doi.org/10.1016/j.jrmge.2015.08.006

Basudhar PK, Saha S, Deb, K (2007) Circular footings resting on geotextile-reinforced sand bed, *Geotextiles and Geomembranes*, **25**, (6), 377–384.

Binquet J, Lee KL (1975) Bearing capacity tests on reinforced earth slabs. *Journal of Geotechnical Engineering Division ASCE*, **101**, (12), 1241–1255.

Biswas A, Krishna AM, Dash SK (2016) Behavior of geosynthetic reinforced soil foundation systems supported on stiff clay subgrade. *International Journal of Geomechanics,* 16**,** 04016007.

Chen Q, Abu-Farsakh M (2014) Ultimate bearing capacity analysis of strip footings on reinforced soil foundation, *The Japanese Geotechnical Society*, **55**, (1), 74–85.

Chen Q, Abu-Farsakh M (2015) Ultimate bearing capacity analysis of strip footings on reinforced soil foundation. Soils Found, 55**,** 74-85.

Chen J, Guo X, Sun R, Rajesh S, Jiang S, Xue J (2021) Physical and numerical modeling of strip footing on geogrid reinforced transparent sand. *Geotextiles and Geomembranes*, *49*(2), 399-412.

Chung W, Cascante G (2007) Experimental and numerical study of soil reinforcement effects on the low-strain stiffness and bearing capacity of shallow foundations, *Geotechnical and Geological Engineering*, **25**, (3), 265–281.

Das BM, Omar MT (1994) The effects of foundation width on model tests for the bearing capacity of sand with geogrid reinforcement, *Geotechnical and Geological Engineering*, **12**, (2), 133–141.

Das BM, Shin EC, Omar MT (1994) The bearing capacity of surface strip foundations on geogrid-reinforced sand and clay—A comparative study. *Geotechnical and Geological Engineering*, *12*(1), 1-14.

Das BM (2019) Advanced Soil Mechanics. Taylor and Francis, New York.

Dash SK, Krishnaswamy NR, Rajagopal K (2001) Bearing capacity of strip footings supported on geocell-reinforced sand, *Geotextiles and Geomembranes*, **19**, (4), 235–256.

Guido VA, Chang DK, Sweeney MA (1986) Comparison of geogrid and geotextile reinforced earth slabs. *Canadian Geotechnical Journal*, **23**, (4), 435–440.

Ghosh A, Bera AK (2005) Bearing capacity of square footing on pond ash reinforced with jute-geotextile, *Geotextiles and Geomembranes*, **23**, (2), 144–173.

Hegde A, Sitharam T (2015) 3-Dimensional Numerical modeling of geocell reinforced sand beds. *Geotextiles and Geomembranes,* 43**,** 171-181.

Huang CC, Tatsuoka F (1990) Bearing capacity of reinforced horizontal sandy ground, *Geotextiles and Geomembranes*, **9**, (1), 51–82.

Kazi M, Shukla SK, Habibi D (2015a) An improved method to increase the load-bearing capacity of strip footing resting on geotextile-reinforced sand bed. *Indian Geotechnical Journal,* 45**,** 98-109.

Khing KH, Das BM, Puri VK, Cook EE, Yen SC (1993) The bearing capacity of a strip foundation on geogrid- reinforced sand, *Geotextiles and Geomembranes*, **12**, (4), 351–361.

Kolbsuzewski J (1948) General investigation of the fundamental factors controlling loose packing of sands. In: Proceedings of the 2nd International Conf Soil Mech Found Eng Rotterdam (4): 47–49

Kumar J, Sahoo JP (2013) Bearing capacity of strip foundations reinforced with geogrid sheets by using upper bound finite-element limit analysis, *International Journal for Numerical and Analytical Methods in Geomechanics*, **37**, (18), 3258–3277.

Latha GM, Somwanshi A (2009) Bearing capacity of square footings on geosynthetic reinforced sand, *Geotextiles and Geomembranes*, **27**, (4), 281–294.

Lee KM, Manjunath VR, Dewaikar DM (1999) Numerical and model studies of strip footing supported by a reinforced granular fill-soft soil system, *Canadian Geotechnical Journal*, **36**, (5), 793–806.

Omar MT, Das BM, Yen SC, Puri VK, Cook EE (1993a) Ultimate bearing capacity of rectangular foundations on geogrid-reinforced sand, *Geotechnical Testing Journal*, **16**, (2), 246–252.

Omar MT, Das BM, Puri VK, Yen SC (1993b) Ultimate bearing capacity of shallow foundations on sand with geogrid reinforcement, *Canadian Geotechnical Journal*, **30**, (3), 545–549.

Patra CR, Das BM, Atalar C (2005) Bearing capacity of embedded strip foundation on geogrid-reinforced sand, *Geotextiles and Geomembranes*, **23**, (5), 454–462.

Raja MNA, Shukla SK (2020) *Geotextiles and Geomembranes*, https://doi.org/10.1016/j.geotexmem.2020.06.005.

Shin EC, Das BM, Lee ES, Atalar C (2002) Bearing capacity of strip foundation on geogrid-reinforced sand, *Geotechnical and Geological Engineering*, **20**, (2), 169–180.

Sitharam TG, Sireesh S (2004) Model studies of embedded circular footing on geogrid-reinforced sand beds, *Proceedings of the Institution of Civil Engineers – Ground Improvement*, **8**, (2), 69–75.

Shukla SK (2004) Discussion of applications of geosynthetics for soil reinforcement by M.I.M. Pinto. Ground Improv 8(4):179–181.

Shukla SK, Yin JH (2006) Fundamentals of Geosynthetic Engineering. Taylor and Francis, London

Shukla, SK (2016) An Introduction to Geosynthetic Engineering, London, CRC Press, Taylor and Francis.

Wang JQ, Zhang LL, Xue JF, Tang Y (2018) Load-settlement response of shallow square footings on geogrid-reinforced sand under cyclic loading. *Geotextiles and Geomembranes,* 46**,** 586-596.

Xu Y, Yan G, Williams DJ, Serati M, Scheuermann A, Vangsness, T (2019) Experimental and numerical studies of a strip footing on geosynthetic-reinforced sand. International Journal of Physical Modeling in Geotechnics, 1-14.

Yetimoglu T, Wu JTH, Saglamer A (1994) Bearing capacity of rectangular footings on geogrid-reinforced sand, *Journal of Geotechnical Engineering*, **120**, (12), 2083–2099.

Zhang L, Wang J, Kaliakin, VN (2020) Load-bearing characteristics of square footing on geogrid-reinforced sand subjected to repeated loading. J. Cent. South Univ. **27,** 920–936. https://doi.org/10.1007/s11771-020-4341-y.

Tables

Table 1 The soil features utilized in tests

Parameter	Value
Cohesion, C (kPa)	12
Specific gravity, G_s	2.68
Residual friction angle, $\phi_{residual}$ (°)	32.3
Peak friction angle, ϕ_{peak} (°)	37. 5
Maximum dry density, γ_{dmax} (kN/m^3)	16.61
Minimum dry density, γ_{dmin} (kN/m^3)	14.09
Dry unit weight, γ_d (kN/m^3)	16.46
Relative density, Dr (%)	90
Mean particle size, d_{50} (mm)	0.34
Effective particle size, d_{10} (mm)	0.20
Maximum particle size, d_{max} (mm)	0.60
Minimum particle size, d_{min} (mm)	0.01
Curvature coefficient, c_c	1.11
Uniformity coefficient, c_u	1.90
Oedometric modulus, E_{oed} (MPa)	30
Fine percentage	9

Table 2 The geogrid's physical properties

Physical Properties of Geogrid CE161	
Polymer	HDPE
Mesh aperture size (mm)	10 x 10
Thickness of mesh (mm)	3.3
Structural weight (gr/m^2)	700
Mechanical features of Geogrid CE161	
Extension at max load (%)	51.7
Tensile strength, max load (kN/m)	6.1
Load at 10% extension (kN/m)	2.9
Tensile strength at strain 5% (kN/m)	1.71
Tensile strength at strain 2% (kN/m)	1.06

Table 3 Experimental setup

Tests No.	Form of reinforcement	N	Placement of the first layer	h/B	L/B or l/L	B (cm)
1	Unreinforced*	0	-	-	-	10
2	Unreinforced*	0	-	-	-	7.5
3	Planar	1	0.3B	-	L=3B	10
4	Planar*	1	0.3B	-	L=5B	10
5	Planar	1	0.3B	-	L=7B	10
6	Planar	2	u = 0.3B	0.4B	L=5B	10
7	Planar	3	u = 0.3B	0.4B	L=5B	10
8	Planar*	1	u = 0.3B	-	L=5B	7.5
9	Planar	2	u = 0.3B	0.4B	L=5B	7.5
10	Planar	3	u = 0.3B	0.4B	L=5B	7.5
11	Semifolded*	1	d=0.2B, D=0.3B	-	l=0.25 L	10
12	Semifolded	1	d=0.2B, D=0.3B	-	l=0.5 L	10
13	Semifolded	1	d=0.2B, D=0.3B	-	l=0.75 L	10
14	Full-folded*	1	d=0.2B, D=0.3B	-	l=1.0 L	10
15	Semifolded	1	d=0.1B, D=0.3B, x_1=0.2B	-	l=0.5 L	10
16	Semifolded	1	d=0.2B, D=0.4B, x_1=0.2B	-	l=0.5 L	10
17	Semifolded	1	d=0.3B, D=0.5B, x_1=0.2B	-	l=0.5 L	10
18	Semifolded	1	d=0.4B, D=0.6B, x_1=0.2B	-	l=0.5 L	10
19	Semifolded	1	d=0.5B, D=0.7B, x_1=0.2B	-	l=0.5 L	10
20	Semifolded	2	d=0.2B, D=0.8B, x_1=0.2B	0.0B	l=0.5 L	10
21	Semifolded	2	d=0.2B, D=1.2B, x_1=0.2B	0.2B	l=0.5 L	10
22	Semifolded	2	d=dopt, D=Dopt, x_1=0.2B	0.4B	l=0.5 L	10
23	Semifolded	2	d=dopt, D=Dopt, x_1=0.2B	0.6B	l=0.5 L	10
24	Semifolded	3	d=0.2B, D=1.2B, x_1=0.2B	0.2B	l=0.5 L	10
25	Semifolded	1	d/B=0.3, D/B=0.6, x_1=0.3B	-	l=0.25 L	7.5
26	Semifolded	1	d=0.3B, D=0.6B, x_1=0.3B	-	l=0.5 L	7.5

27	Semifolded	1	d=0.3B, D=0.6B, x_1=0.3B	-	*l*=0.75 L	7.5
28	Full-folded	1	d=0.3B, D=0.6B, x_1=0.3B	-	*l*=1.0 L	7.5
29	Semifolded	1	d=0.2B, D=0.4B, x_1=0.2B	-	*l*=0.75 L	7.5
30	Semifolded	1	d=0.3B, D=0.6B, x_1=0.3B	-	*l*=0.75 L	7.5
31	Semifolded	1	d=0.4B, D=0.8B, x_1=0.4B	-	*l*=0.75 L	7.5
32	Semifolded	1	d=0.5B, D=1.0B, x_1=0.5B	-	*l*=0.75 L	7.5
33	Semifolded	2	d=0.2B, D=0.8B, x_1=0.2B	0.0B	*l*=0.5 L	7.5
34	Semifolded	2	d=0.2B, D=0.8B, x_1=0.2B	0.2B	*l*=0.5 L	7.5
35	Semifolded	2	d=0.2B, D=1.0B, x_1=0.2B	0.4B	*l*=0.5 L	7.5
36	Semifolded	2	d=0.2B, D=1.2B, x_1=0.2B	0.6B	*l*=0.5 L	7.5
37	Semifolded	3	d=0.2B, D=1.2B, x_1=0.2B	0.2B	*l*=0.5 L	7.5

N= number of reinforcing layers, x_1= thickness of the folded geogrid reinforcing layer, d=depth of lap element, D= total embedment of geogrid layers, h= vertical spacing between geogrid folded layers, *l*= length of lap and overlap elements, L=length of a geogrid layer in planar or folded, u=embedment of the first layer, B= footing width, and signs (*) mean to repeated each test two following times.

Table 4 Results of the strip footing test for footing width (B=10 cm and B=7.5 cm) in both unreinforced and planar reinforced soils.

B (cm)	L/B	Number of tests	N	u/B	q_u (kPa)	BCR
10	0	1	0	-	330	1.00
10	3	2	1	0.3	440	1.33
10	5	3	1	0.3	487	1.48
10	7	4	1	0.3	425	1.29
7.5	0	5	0	-	280	1.00
7.5	3	6	1	0.3	310	1.11
7.5	5	7	1	0.3	365	1.30
7.5	7	8	1	0.3	308	1.10

Table 5 Results of the strip footing test for two footing widths (B=10 cm and B=7.5 cm) in both unreinforced and planar reinforced soils.

B (cm)	L/B	N	u/B	*h*/B	q_u (kPa)	BCR
10	0	0	-	-	330	1.00
10	5	1	0.3	-	487	1.48
10	5	2	0.3	0.4	530	1.61
10	5	3	0.3	0.4	550	1.67
7.5	0	0	-	-	280	1.00
7.5	5	1	0.3	-	365	1.30
7.5	5	2	0.3	0.4	390	1.39
7.5	5	3	0.3	0.4	415	1.48

Table 6 Results of the strip footing test for footing width (B=10 cm) in both unreinforced and geogrid folded reinforced soils

B (cm)	L/B	*l*/L	u/B	d/B	q_u (kPa)	BCR_l	BCR_f
10	5	-	0.3	-	487	1.00	1.47
10	5	0	0.3	0.2	490	1.01	1.48
10	5	0.25	0.3	0.2	500	1.03	1.52
10	5	0.5	0.3	0.2	510	1.05	1.55
10	5	0.75	0.3	0.2	511	1.05	1.56
10	5	1	0.3	0.2	520	1.07	1.58

Table 7 Results of the strip footing test for footing width (B=10 cm) in both planar and geogrid folded reinforced soils

B (cm)	Form of layer	No. of layers	l/B	h/B	d_2/B	q_u (kPa)	BCR_l	BCR_f
10	-	-	-	-	-	330	-	1.00
10	Planar	2	0.5	0.4	-	530	1.09	1.61
10	Planar	3	0.5	0.4	-	550	1.13	1.67
10	Folded	2	0.5	0.0	0.6	732	1.50	2.22
10	Folded	2	0.5	0.2	1	690	1.42	2.09
10	Folded	2	0.5	0.4	1.6	667	1.37	2.02
10	Folded	3	0.5	0.0	1	734	1.51	2.22

Figures

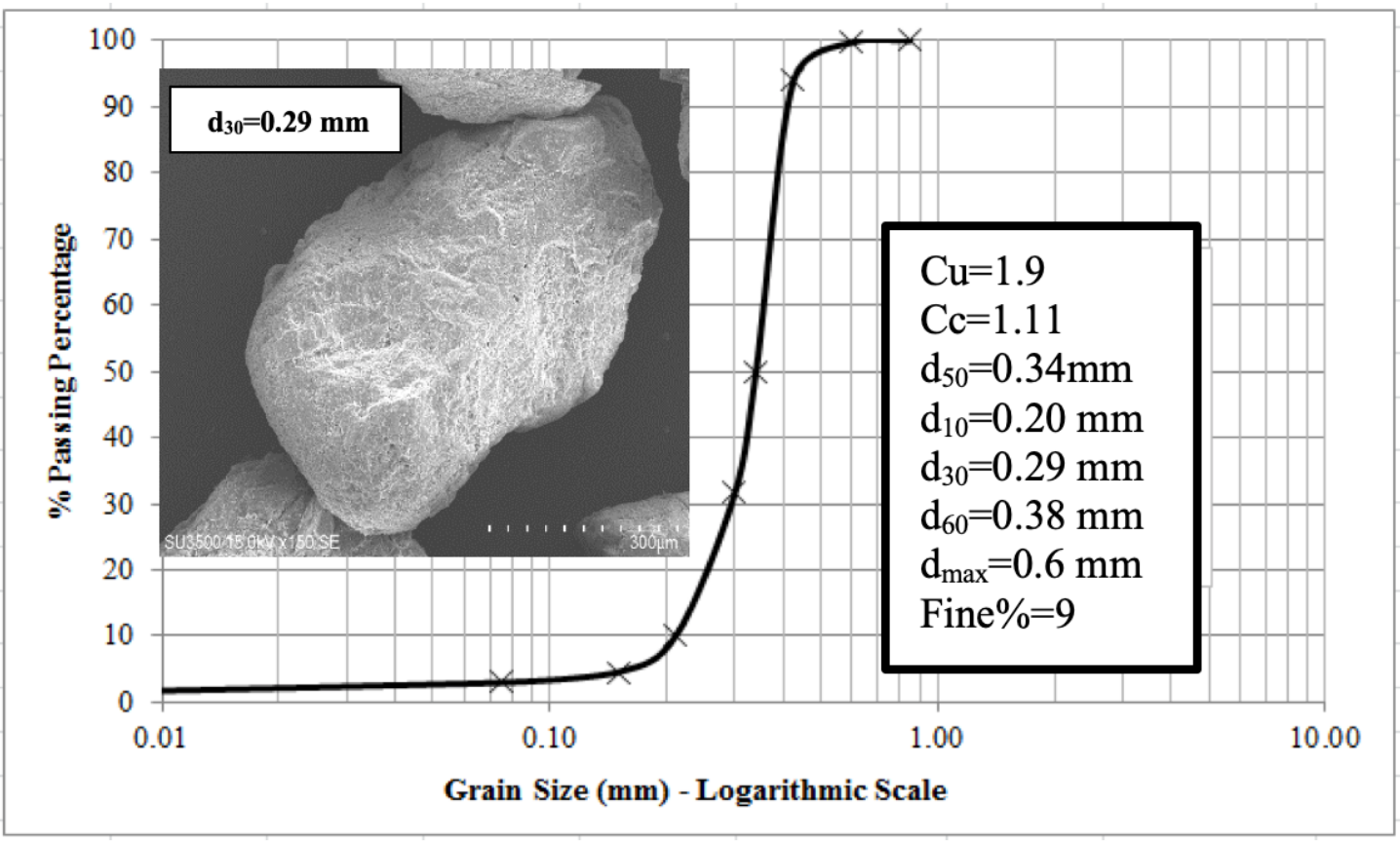

Figure 1

Particle size distribution analysis

Figure 2

SEM analysis of the particle size of fine sand

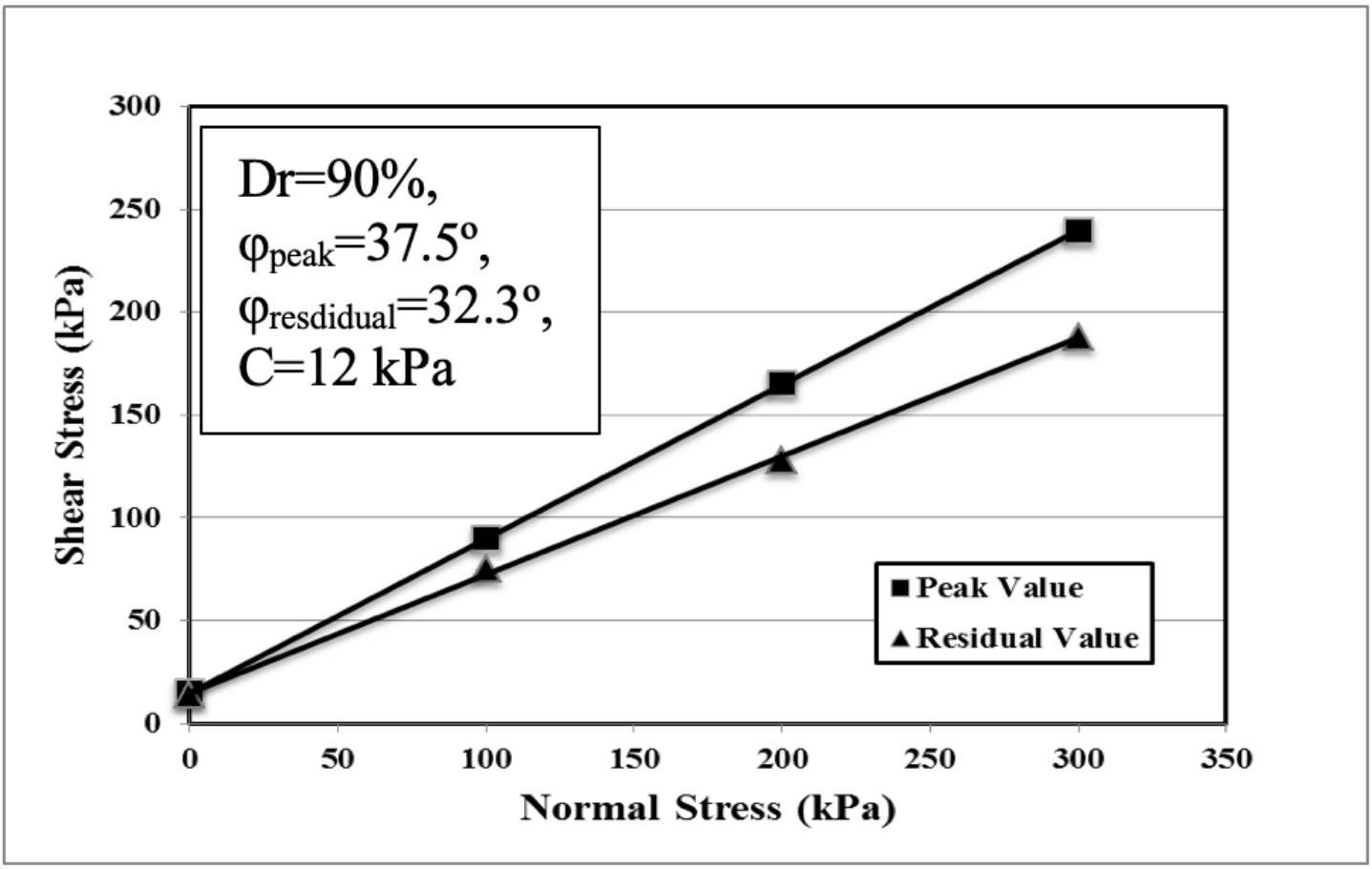

Figure 3

Mohr–Coulomb envelope curve on Firozkoh fine sand

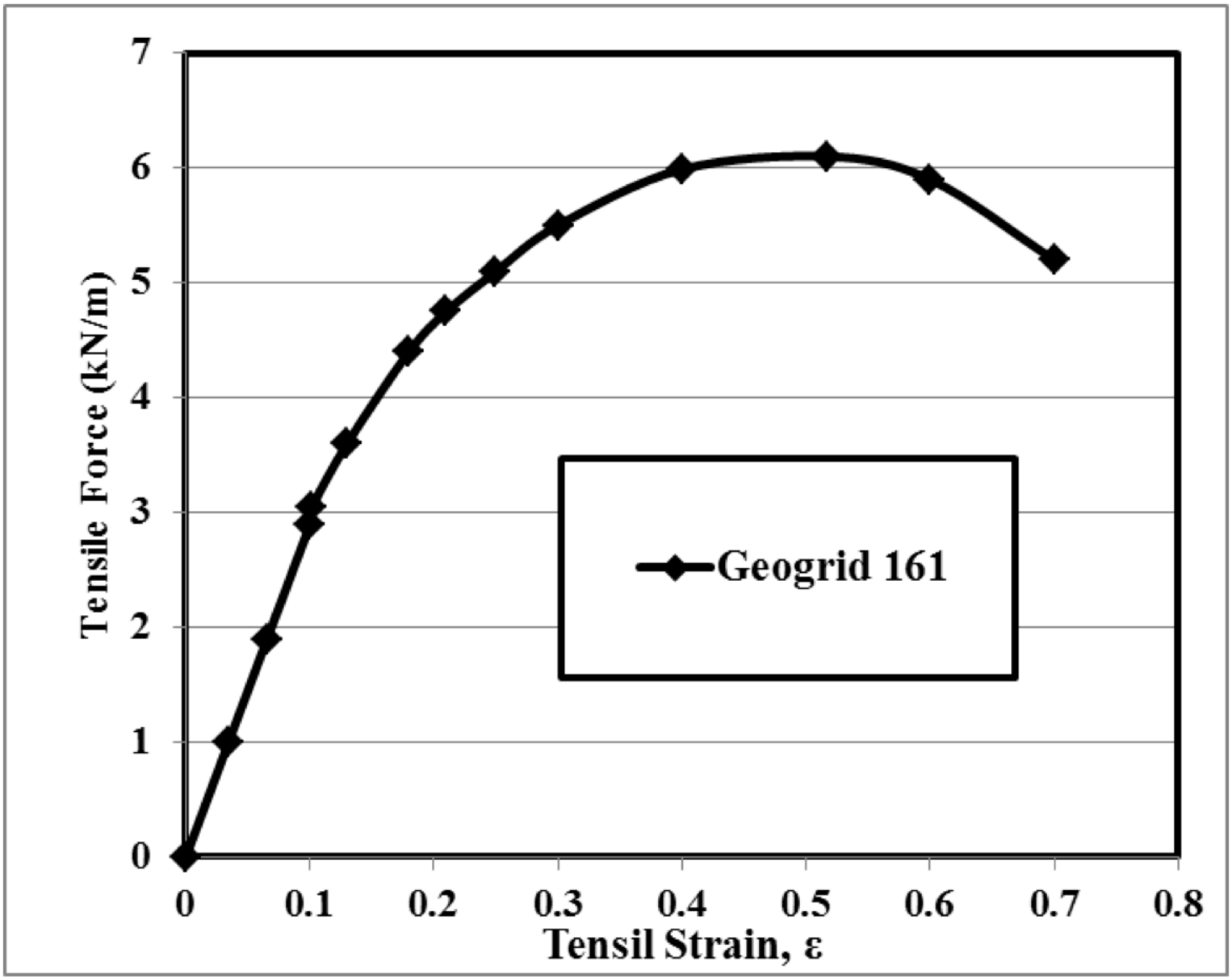

Figure 4

The tensile force-strain curve of geogrid CE161

Figure 5

a) Illustration of the physical device, b) Image of laboratory model tests

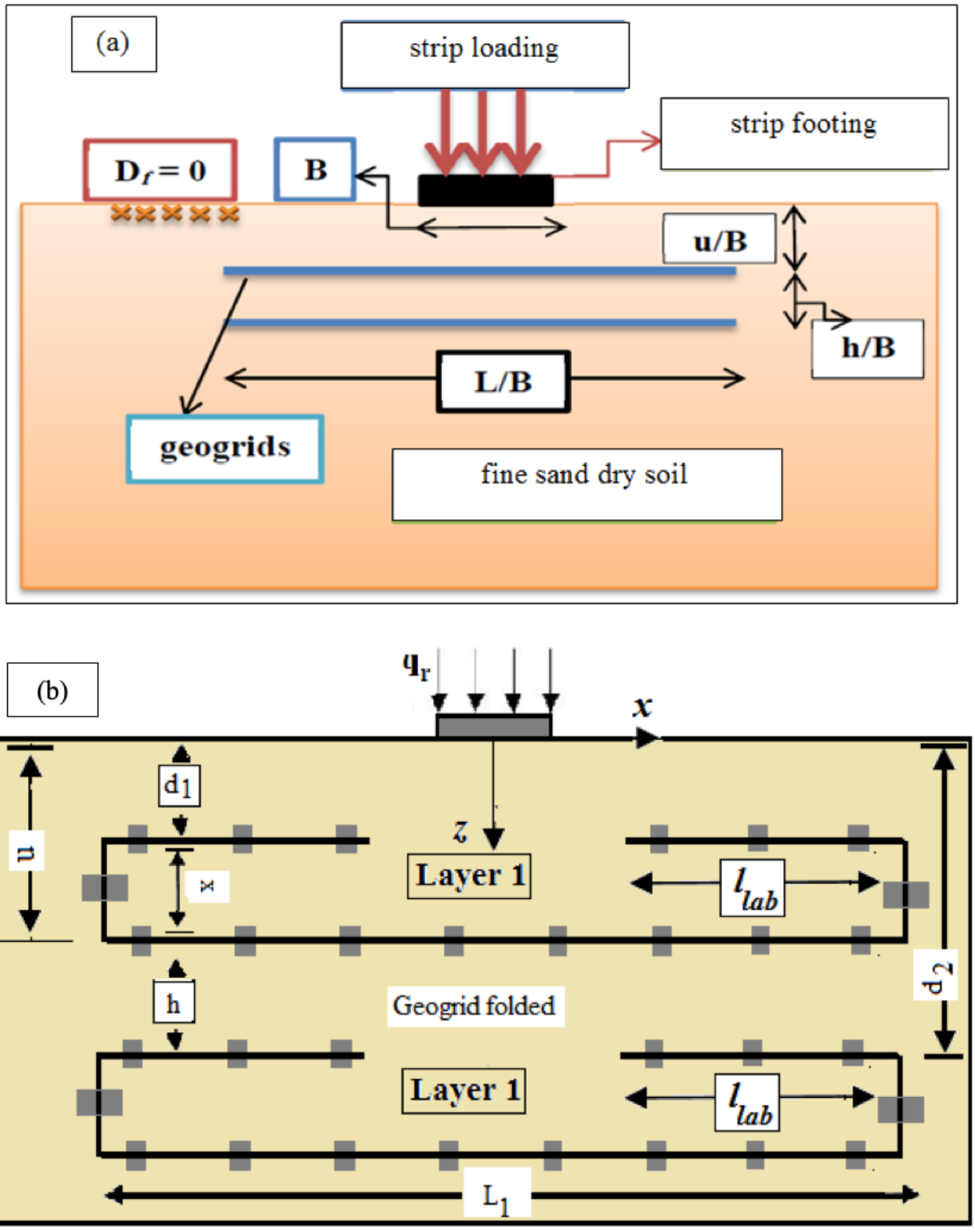

Figure 6

Illustration of the geogrid arrangement, a) layout of reinforcing planar arrangement, and b) layout of reinforcing folded arrangement

Figure 7

Performance of one-layer geogrid-reinforced sand for different lengths of reinforcing planar arrangement: (a) B=10 cm, (b) B=7.5 cm

Figure 8

The employed stress-relative settlement for multiple layers, B=10 cm

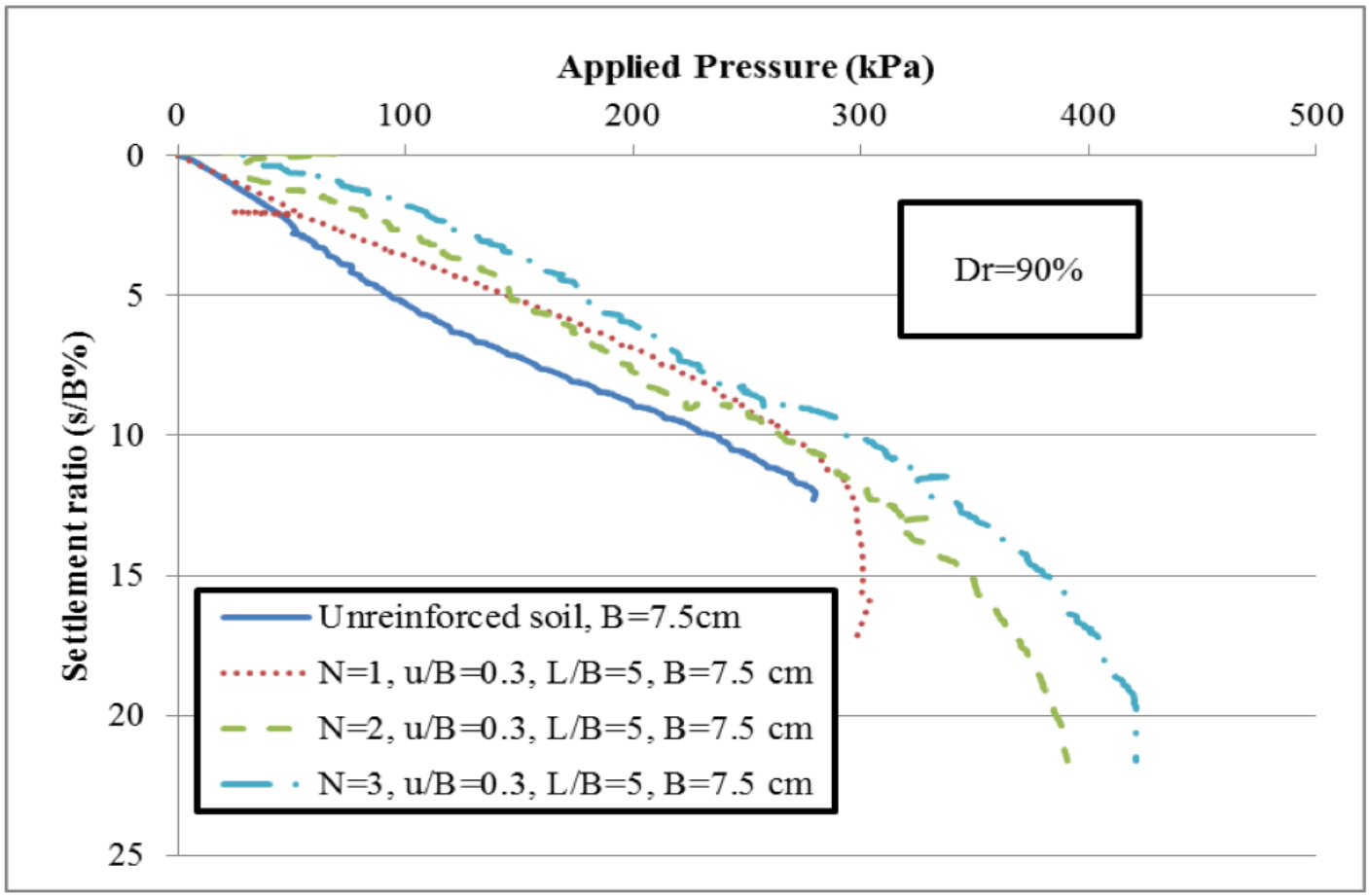

Figure 9

The employed stress-relative settlement for multiple layers, B=7.5 cm

Figure 10

The failure mode of (a) one geogrid planar layer and (b) one geogrid folded layer

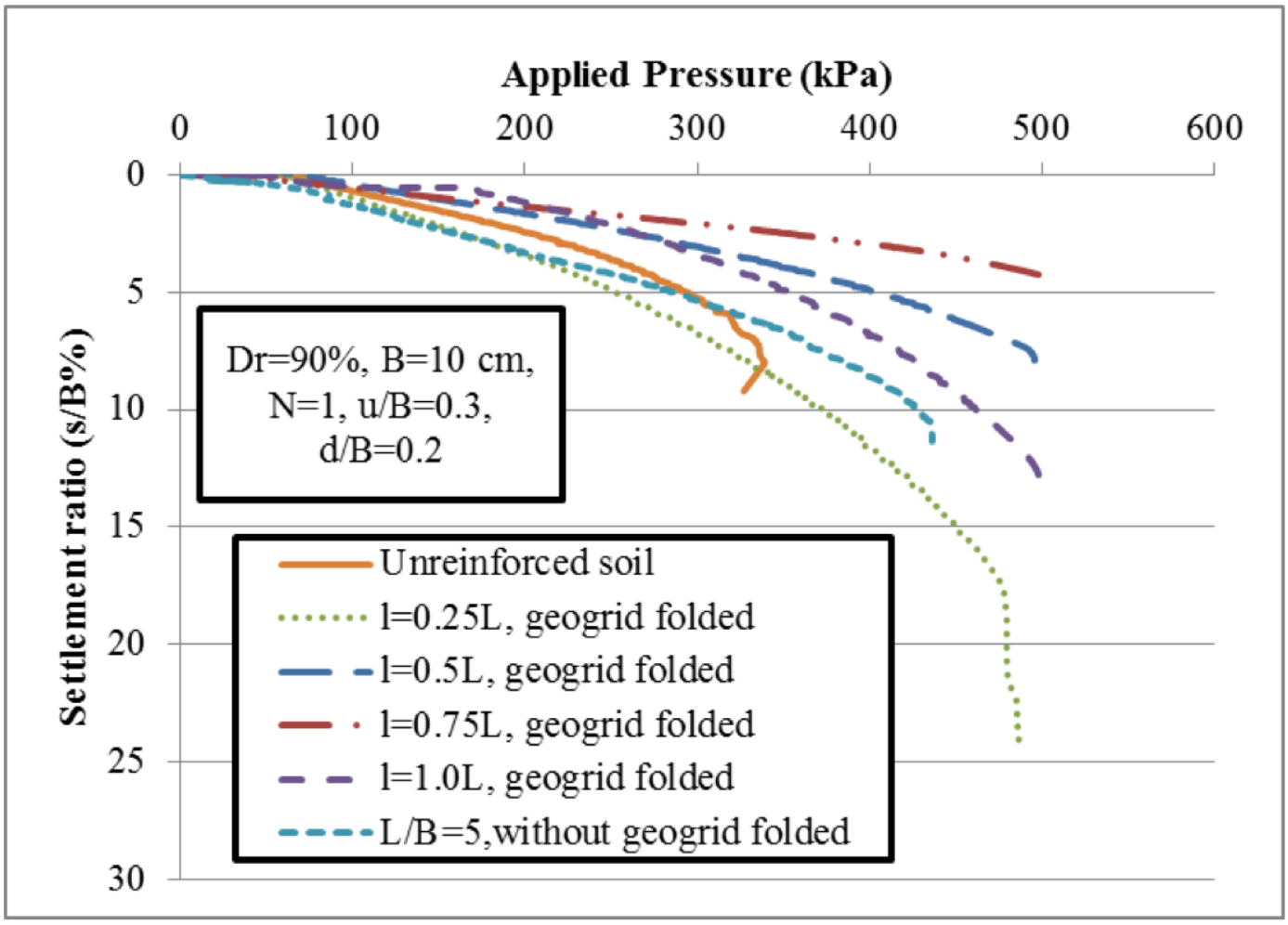

Figure 11

Behavior of a one-layered geogrid folded for various lap lengths

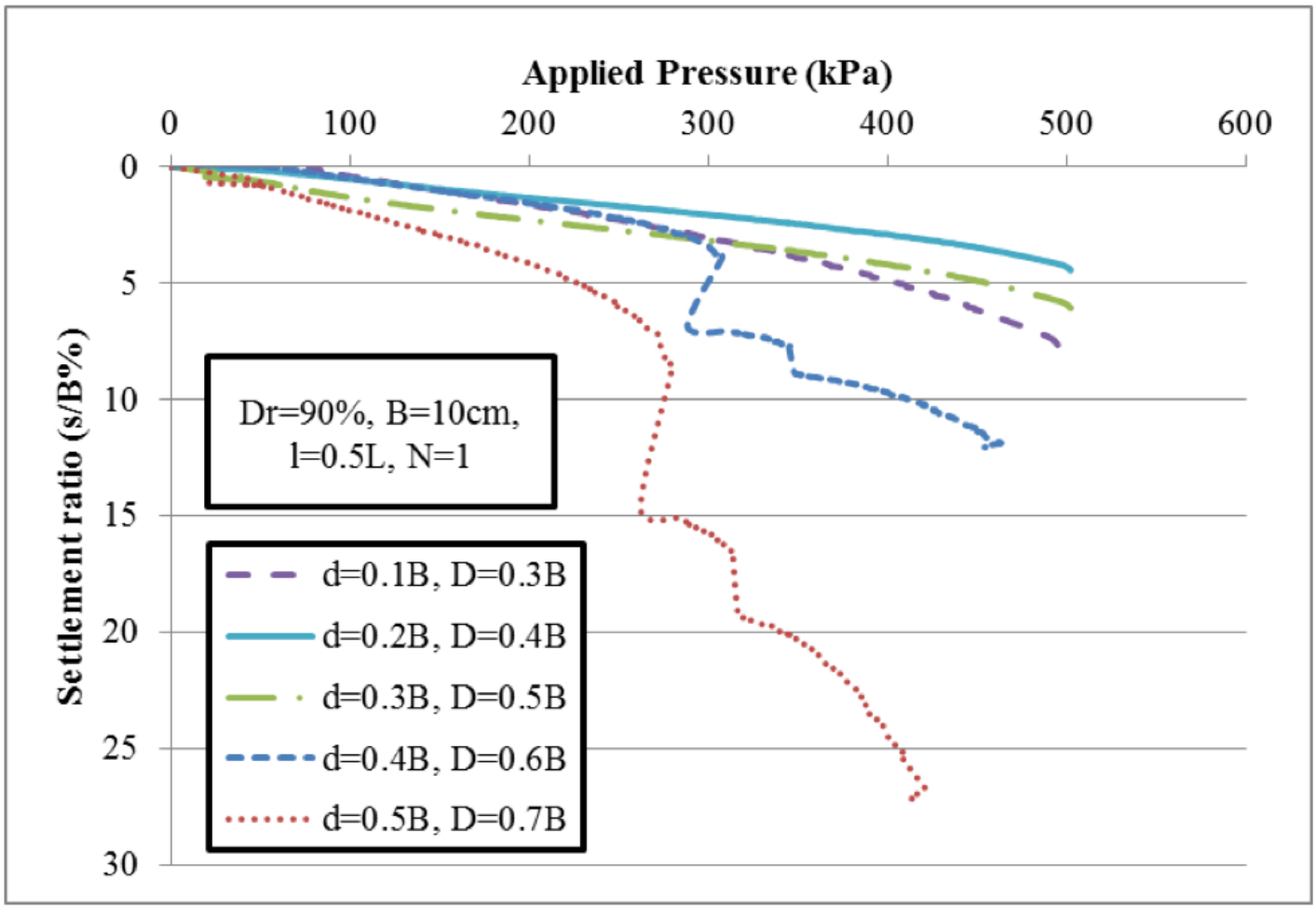

Figure 12

Behavior of a one-layered geogrid folded for various embedment depths

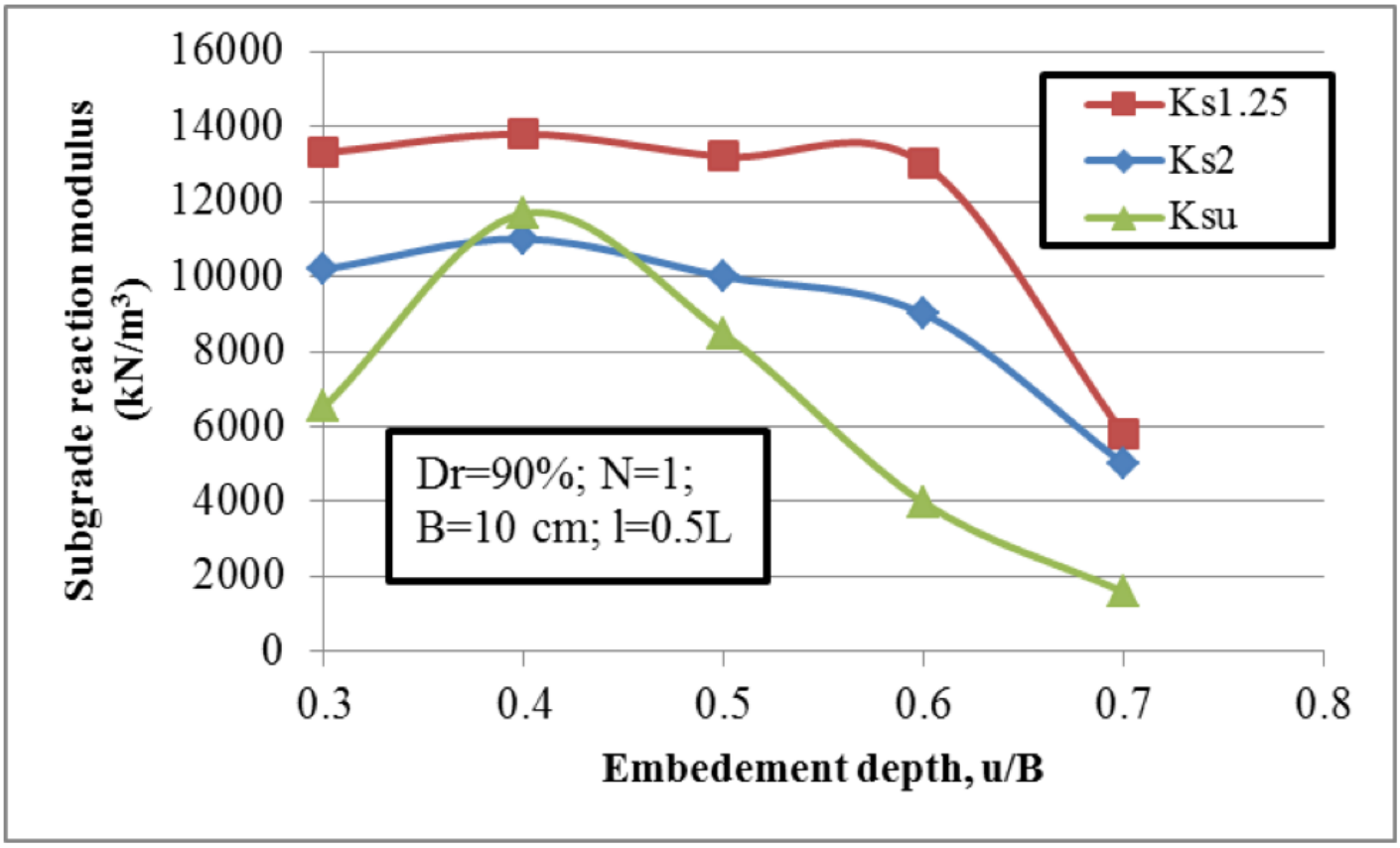

Figure 13

Variation in the subgrade reaction modulus with embedment depth ratio

Figure 14

Variation in the impact factor with the embedment depth ratio

Figure 15

Behavior of multilayered geogrids folded for various spacing ratios (h/B)

Figure 16

BCR versus spacing ratio (h/B) between geogrid folded layers

Figure 17

Behavior of multilayered geogrids folded for various embedment depths

Figure 18

Effect of footing width on lap lengths

Figure 19

Failure mode in geogrid semifolded reinforced sand for footing width B=7.5 cm, a) before loading, b) after loading

Figure 20

Effect of footing width on the behavior of a multilayered geogrid folded for B=7.5 cm with a) various embedment depths, b) various spacing ratios (h/B), B=7.5 cm